AFOSR 2763

THE UNIVERSITY OF MICHIGAN

COLLEGE OF ENGINEERING
Department of Chemical and Metallurgical Engineering

Technical Note

KINETICS OF SINTERING OF RUTILE SINGLE CRYSTAL SPHERES

H. M. O'Bryan, Jr.
G. Parravano

ORA Project 02832

under contract with:

UNITED STATES AIR FORCE
AIR RESEARCH AND DEVELOPMENT COMMAND
AIR FORCE OFFICE OF SCIENTIFIC RESEARCH
CONTRACT NO. AF 49(638)-493
PROJECT NO. 9762, TASK NO. 37621
WASHINGTON, D.C.

administered through:

OFFICE OF RESEARCH ADMINISTRATION ANN ARBOR

July 1962

TABLE OF CONTENTS

LIST OF ILLUSTRATIONS

LIST OF ILLUSTRATIONS (Concluded)

ABSTRACT

The sintering of single crystal rutile has been studied in air and in reducing atmosphere in the temperature range 900 to 1350°C using a sphere-to-sphere model. Rate data show that there are two sintering periods: a slow initial growth characterized by a rate exponent n = 7 and a more rapid subsequent period n = 2. The development of flat surfaces or facets on the particles is used to explain the two periods. A scaling exponent of 3 and an activation energy of 70 kcal/mole indicate that volume diffusion is the sintering mechanism. The initial rate exponent cannot be explained. Increase sinterability of reduced rutile is explained by the defect structure. Facet formation on rutile spheres is discussed.

INTRODUCTION

This report discusses some problems related to changes in the configuration of solids as they proceed toward the equilibrium shape and size. These problems have been studied extensively during the past fifteen years in metallic systems because of the practical interest of understanding and controlling the sintering of particulate aggregates. The data obtained from powdered samples represent geometrically complicated phenomena and the formulation of sintering kinetics is all but impossible in these systems. The simple geometric models of two spheres in contact or a sphere-on-a-plate have been proposed to permit interpretation of the data.[1] Many data have been gathered for the metal systems using these models. Recently these techniques have been applied to ceramic materials to determine their sintering behavior.

Previous investigations on the welding of single crystal microspheres of rutile have shown that the value of the exponent n in the expression describing the rate of growth of the circular contact area between spheres

$$x^n = kt \qquad (1)$$

where x is the contact radius, k is a constant, and t is time, has a value of about 2.[2] This value was averaged from about 50 experimental runs, performed in air and reducing atmospheres in the temperature range 900 to 1350°C with microspheres of 1.0 mm diameter and for intervals of time corresponding to about 30% neck formation (with respect to sphere diameter).

To understand better the nature of the transport process responsible for the reported value of n in expression (1), we have subjected the system to additional investigations. In particular, attention has been directed toward examining the initial period of sintering, with the intent of bringing to light the effect on the sintering rate of flat surfaces formed on the spherical surface in the neck region during sintering. If a topographical factor were responsible for the value of n = 2, a study of sintering during the initial stage, when the neck region is still bound by curved surfaces, should prove revealing, since it would be reflected in a different numerical value for n in Eq. (1). In addition, it has been shown that a change of scale of the system can be used to differentiate between mechanisms of mass transport in solids.[3] Thus the times to effect geometrically similar changes are related by an expression of the form

$$t_1 = \lambda^m t_2 \qquad (2)$$

where λ is the ratio of a characteristic dimension of system 1 to the similar dimension in system 2. The exponent m in Eq. (2) can be used as a criterion to elucidate the mechanism of transport during contact formation.

As it will be apparent from the results reported below, the geometrical conditions in the contact area play a critical role in fixing the value of n and in controlling the transport process in both the value of its rate and in its rate expression.

EXPERIMENTAL SYSTEM

The chemical composition of the initial rutile single crystals, the preparation of the rutile microspheres, the equipment used for recording the increase in neck width as a function of time, and the procedure followed for obtaining and treating the experimental data have been discussed in detail previously.[2]

The microspheres, 0.5 to 1.3 mm diameter, were mounted in a platinum groove, electrically heated, and set directly in the field of an optical microscope. A filar stage in the microscope eyepiece enabled measurement of changes in neck size as a function of time at sintering temperatures. A stream of air or mixtures of H_2O+H_2 was slowly passed through the hot stage during sintering measurements.

RESULTS

Direct evidence for the formation of facets on TiO_2 spheres is shown in Fig. 1. The facets formed in air appeared smooth, while those developed under reducing conditions appeared covered with minute striations (Fig. 2). More severe heating in reducing conditions caused the striations to become smoothed (Fig. 3). In addition, whisker growth was observed on many areas of the surface of the spheres. The effect of temperature on the rate of welding of microspheres, in air, is shown in Figs. 4 and 5. Similar results obtained under reducing conditions ($p_{H_2}/p_{H_2O} = 10$) are presented in Figs. 6 and 7. Comparison between the data shows that the sintering rate at 1100°C is about 40 times faster under reducing conditions than in air (Fig. 8). As is apparent from these figures, a distinct change in sintering rate occurs at $x/a = 0.075$ to 0.1. The time at which the change in rate occurs, t_c, is strongly dependent upon the temperature of sintering. Two different periods of sintering can, then, be recognized: an initial one, characterized by a relatively slow rate followed by a period of more rapid sintering. The rate exponents, n from

Eq. (1), calculated from the experimental data for both sintering stages for some 100 runs on 1.0 mm diameter spheres, are presented in Table I. A rate exponent n = 7 is seen to fit the data for the initial period while n = 2 is the rate exponent calculated for the second sintering period.

From sintering times to reach ratios x/a = 0.07 and x/a = 0.25 at different temperatures, an activation energy of 70 ± 10 kcal/mole was computed for each period for both atmospheres. Figure 9 shows the results for air, while Fig. 10 shows the results for p_{H_2}/p_{H_2O} = 10. To determine the effect of scale on sintering rates, experiments have been performed with spheres with diameters varying between 0.5 and 1.3 mm. Despite a large amount of scattering, it is possible to limit the value of a scaling exponent of m = 3 for the second stage of sintering (Fig. 11).

Weight loss for severely faceted and extensively sintered spheres (5 hours, 1100°C in reducing conditions) was < 0.25%. X-ray analyses on spheres sintered in both types of atmosphere indicated that the rutile structure was retained. No change in center-to-center distance between unsintered and sintered sphere pairs was detected. The angle of contact between the sphere surface and the neck decreased with extent of sintering.

A word should be said about the reproducibility of the experimental data. In nearly all cases sintering sphere pairs showed a slow initial period (rate exponent n ≈ 7) followed by a rapid period (rate exponent n ≈ 2). The change in rate exponent occurred at a geometrically similar neck size x/a = 0.07 to 0.1. However, these rate features were often displaced along the time axis. Thus two pairs of spheres sintered under identical conditions might show at 1100°C a 50-minute difference in the time to reach x/a = 0.3 for a total sintering time of 400 minutes. It was also observed that the facet formation showed varying orientation with respect to the contact neck.

DISCUSSION OF THE EXPERIMENTAL RESULTS

Four possible mechanisms for the transport of mass which occurs during sintering have been suggested: evaporation-condensation, viscous or plastic flow, surface diffusion, and volume diffusion. To determine the transport process involved for a particular material it is necessary that the sintering data yield rate expressions, change of scale effects, center-to-center shrinkage, activation energies, and characteristic constants which are consistent with one of the four possible mechanisms.

The significant data presented in the previous section which must be correlated are:

TABLE I

TIME DEPENDENCE OF THE VALUE OF n IN EQUATION (1) FOR RUTILE SPHERES

(1 mm diameter)

Atmosphere	Temperature, °C	Inverse Slope, n	
		Initial Stage	Subsequent Stage
Air	1000	-	1.6
	1050	7.5 ± 1.0*	2.2 ± 0.8
	1100	7.2 ± 0.3	1.5 ± 0.3
	1150	8.0	1.6
	1200	-	1.7 ± 0.1
	1250	6.1 ± 1.0	1.7 ± 0.1
	1300	7.6	1.5
	1350	6.0	1.5
Reducing Atmosphere, $p_{H_2}/p_{H_2O} = 10$	900	5.6	2.1 ± 0.1
	950	8.6 ± 0.5	2.5 ± 0.5
	1000	7.3 ± 0.6	1.9 ± 0.2
	1050	7.6 ± 1.4	1.9 ± 0.1
	1100	6.0 ± 1.2	2.0 ± 0.1
	1150	-	2.3 ± 0.2
	1200	-	1.9

*Tolerance limits are for one standard deviation.

(1) The value of n is dependent upon the extent of sintering: for $t < t_c$, $n \approx 7$, while for $t > t_c$, $n \approx 2$.

(2) The change from one value to the other occurs over a narrow range of the ratio $x/a (\approx 0.075)$.

(3) The values of the activation energy for sintering when $t < t_c$ and $t > t_c$ are similar.

(4) No change of center-to-center distance between the sintering spheres can be detected.

(5) In the course of sintering, rutile microspheres develop rather flat facets on their surface, the time of appearance of facets being strongly influenced by the temperature.

(6) A scaling exponent of $m \approx 3$ is obtained.

(7) Reduced oxygen pressure increases sintering rate.

The rate expressions which have been derived for the growth of the contact area between particles are based on a spherical model.[1] Whenever flat regions develop in the neck area, this model becomes invalid, since the presence of facets introduces a different neck geometry. Therefore, in the present discussion of the experimental results we shall consider two different situations in the neck region of the welding microspheres: (1) without the presence of facets; (2) with the presence of flat surfaces.

Initially, the former situation occurs, but as sintering progresses and facets appear on the surface of the microspheres, the latter case should be considered. Thus, the sintering rate expression changes as facets develop. We suggest that the sharp, consistent break in the plots of the experimental points (Figs. 7 to 10) is the result of the change of the rate expression for sintering rather than a change in mechanism. In addition, the strong temperature dependence of t_c is consistent with the assumption that the value of t_c is connected with a solid state rearrangement of the type involved in facet formation. Since the change in rate expression always occurs at similar amounts of sintering, it would seem that the transport mechanism responsible for sintering in the initial period is also responsible for the rearrangement required to produce the facets.

For $t < t_c$, sintering occurs between rutile microspheres which still retain their spherical characteristics in the neck region. The experimental results show that the value of the rate exponent n is ≈ 7. According to previous derivations,[1] this fact would indicate that transport by surface diffusion was prevalent. The corresponding rate expression is:

$$\left(\frac{x}{a}\right)^7 = \frac{16}{7}\frac{D_s\gamma\Omega^2 t n_s}{a^4 kT} . \qquad (3)^*$$

Taking a = 0.05 cm, $\gamma = 10^3$ ergs/cm^2, $\Omega = 10^{-23}$ cm^3/atom, $n_s = 10^{14}$ atom/cm^2, and using the experimental results for x/a = 0.08 at t = 600 sec and T = 1100°C (Fig. 6), a value for D_s = 1.2 cm^2/sec can be calculated for sintering in reducing atmosphere. For a similar amount of sintering in air at the same temperature, we find $D_s = 3.0 \times 10^{-2}$ cm^2/sec.

These results, together with the observation that no change in the center-to-center distance was detected during sintering, would indicate that surface diffusion is a predominant mechanism of mass transport. The operation of a diffusion mechanism is strengthened by the large effect of the atmosphere on the rate of neck growth. At 1100°C, the ratio of the diffusion coefficient in air to that in p_{H_2}/p_{H_2O} = 10 is about 1/40.

Although the exact nature of the diffusing species is unknown, from the evidence of other studies on the Ti-O system the identity of the mobile species can be inferred. It has been shown that the stoichiometric defect in rutile consists of trivalent cations and vacant anion lattice positions.[4] Thus the number of anion vacancies is an inverse function of oxygen pressure. Metal oxidation studies generally indicate oxygen-ion diffusion is the rate-controlling process.[5] Our data, which show that at 1100°C the ratio of the diffusion coefficient in air to that in p_{H_2}/p_{H_2O} = 10 is about 1/40, are consistent with a sintering rate controlled by oxygen-ion diffusion.

From recent measurements of oxygen diffusion in single crystals of rutile[6] it is possible to calculate the value of the volume diffusion of oxygen at 1100°C in air. When this is done, a value of $D_V = 2.6 \times 10^{-12}$ cm^2/sec is found. Since, generally, the difference between surface- and volume-diffusion coefficients would at most amount to four or five orders of magnitude, the values of the former obtained through the application of Eq. (3) are not consistent with a mechanism involving the diffusion of oxygen ions along the surface. A mechanism based on volume diffusion would remove part of this inconsistency. In fact, the value of D_V, calculated from the volume-diffusion rate expression

$$\left(\frac{x}{a}\right)^5 = \frac{40 D_V \gamma\Omega\pi t}{a^3 kT} \qquad (4)$$

using our results obtained at 1100°C, in air, is $D_V = 2.0 \times 10^{-9}$ cm^2/sec. This suggestion is strengthened by the fact that the derived activation energy for this period of sintering (~70 kcal/mole) is similar to the value obtained

*Symbols are identified in Appendix D.

from direct anion diffusion measurements (73 kcal/mole).

Since no scaling data are available for sintering during the initial period, this criterion cannot be used to determine the identity of the diffusion mode. The failure to observe a shrinkage in the center-to-center distance for sintering sphere pairs may not be a rigorous denial of volume-diffusion transport, since the amount of shrinkage which might be observed is so small as to be unnoticed during the rather short initial rate period.

For $t > t_c$, sintering occurs between rutile microspheres which have developed flat facets. The experimental results show that the rate exponent has a value $n \approx 2$. A previous derivation attributes this value to mass transport by a plastic or viscous flow mechanism.[1] However, rutile is a crystalline solid and the stresses which surface tension might develop in the neck region would hardly be sufficient to cause deformation. Hence the flow mechanism cannot be a large contributing factor in rutile for the conditions studied.

The activation energies for this second period are similar to those derived for the first period (Figs. 9 and 10). The experimental scaling exponent ($m \approx 3$) would suggest a volume-diffusion mechanism. A previous derivation for sintering by volume diffusion in the presence of flat surfaces at the neck has been used to explain the growth of the contact neck at Al_2O_3 spheres in dry hydrogen for the temperature range 1825°C-2000°C.[7]

The derived expression

$$\frac{(x-x_o)^3}{a^3} = \frac{3k_2\gamma\Omega}{kTa^3} D_v \cos\left(\frac{\alpha}{2}\right)(t - t_o) \qquad (5)$$

shows a rate exponent of $n \approx 3$ (scaling exponent $m = 3$), and because the interparticle grain boundary is the material source, a shrinkage in center-to-center distance is required. The first and third requirements indicate this rate expression is not applicable to our data.

Rate expressions for the sintering of rutile spheres after the development of facets have been derived assuming various types of facet movements. Both volume- and surface-diffusion mass transport mechanisms were considered, but no expression was found which could accommodate the $n = 2$ rate exponent, the $m = 3$ scaling factor, and the lack of shrinkage. (See Appendices A-C.) An empirical expression for the rate of contact area growth after facet formation has the form

$$\left(\frac{x}{a}\right)^2 = \frac{kD\Omega\gamma t}{a^3 kT} . \qquad (6)$$

Assuming a k value of 100, volume-diffusion coefficients can be calculated from the data at 1100°C to be $D_V = 4 \times 10^{-6}$ cm^2/sec for air and $D_V = 1.7 \times 10^{-4}$ cm^2/sec in reducing atmosphere. These coefficients are considerably higher than those calculated from the literature or those calculated from the literature or those calculated for the initial period.

In light of the predominant evidence for diffusion, the difficulty of reproducing experimental data along the time axis can be interpreted as caused by the anisotropy of the tetragonal rutile crystal structure. Diffusion coefficients in such a lattice would be expected to vary with the crystallographic direction. The orientation of facets can be generally coordinated with the time displacement.

Mass transport by an evaporation condensation mechanism is unlikely. The data yield neither the appropriate rate exponent nor the correct scaling exponent for this mechanism. From the free energy functions for gaseous rutile[8] and for solid rutile[9] the vapor pressure equation can be calculated

$$\ln p = -139700/RT + 18.6 \qquad (1800\text{-}2300°K). \qquad (7)$$

It is seen that this vaporization energy is 70 kcal/mole higher than the observed activation energy for sintering while the vapor pressure at 1800°K is six orders of magnitude lower than that required to give the sintering rates observed at 1350°C.

CONCLUSIONS

While the data indicates that a diffusional transport of matter is operative in rutile sintering, the exact mode of diffusion is not completely clear. The kinetics of contact area growth in the initial period point to a mechanism controlled by surface diffusion. However, the value of the activation energy for both the initial and subsequent periods, the value of the initial-diffusion coefficient, and the exponent of the scaling ratio are more directly related to a volume-diffusion process. The oxygen pressure dependence and the activation energy of the sintering indicate that oxygen-ion migration is the rate-controlling step in the diffusion process.

Although previous work on the sintering of ice spheres disclosed abnormally high diffusion coefficients using Eq. (3), it was concluded that surface diffusion was the predominant process.[10] In rutile, there is similarly an unusually high coefficient for volume diffusion as calculated by Eq. (7). This fact might be explained if development of facets provides preferred diffusion pathways. The rate of facet formation is comparable with the rate of change-over from the first to the second stage of sintering. This can be taken as an indication that a similar transport process is fundamental to both effects.

APPENDIX A

CALCULATION OF SINTERING DRIVING FORCE ASSUMING SURFACE-VAPOR EQUILIBRIUM

Imagine a three-step process in which a mass of material, dm, on a solid body composed of two surfaces, 1 and 2, is:

(1) evaporated from surface 1;

(2) transported somehow to surface 2; and

(3) deposited at surface 2.

If boundary processes are rapid, it is obvious that steps 1 and 3 involve no free energy change and that the total free energy change may be expressed as

$$dF = \frac{dm}{M} (F_2 - F_1)$$

where F is molal free energy. The corresponding decrease in total surface energy is:

$$dF = \gamma_2 dA_2 + \gamma_1 dA_1 .$$

Now

$$F_1 = \mu_1 = RT \ln f_1 + B$$

$$F_2 = \mu_2 = RT \ln f_2 + B$$

$$f_2 = p_2$$

$$f_1 = p_1$$

where the standard state is vapor at 1 atm at the temperature in question.

Thus

$$\gamma_2 dA_2 + \gamma_1 dA_1 = \mathring{A} \frac{dm}{M} (\mu_2 - \mu_1) = \frac{dm}{M} \mathring{A} RT \ln \frac{p_2}{p_1} .$$

Now if surface 1 is close to equilibrium, i.e.,

$$p_1 \cong p_o, \quad u_1 \cong u_o, \quad \text{and} \quad u_2 = \mu - \mu_h$$

$$\gamma_2 dA_2 + \gamma dA_1 = \mathring{A} \frac{dm}{M} (\mu_2 - \mu_o) = \mathring{A} \frac{dm}{M} (\mu - \mu_h - \mu_o).$$

Since $dm = \rho dV$ where ρ is the density

$$\mu - \mu_h - \mu_o = \frac{M(\gamma_2 dA_2 + \gamma_1 dA_1)}{\mathring{A} dV \rho}$$

$$\Omega = \frac{M}{\mathring{A}\rho}$$

$$\mu - \mu_h - \mu_o = \frac{(\gamma_2 dA_2 + \gamma_1 dA_1)}{dV} .$$

Since this expression is similar to that derived under conditions of surface volume equilibrium,[3] we conclude that for calculations of boundary values of the chemical potentials, conditions involving equilibria between volume, surface and gas phases lead to a similar result.

APPENDIX B

FACET FORMATION ON CURVED SURFACE

Due to the difficulties of nucleation on flat surfaces, the development of the facet will preferably occur by inward displacement.[11] Consider a circular, flat facet which forms on a spherical surface by removal of material from the top of the facet or the addition of material around the perimeter of the facet. Our first concern will be with the process of formation of a flat plane on a curved surface. In Fig. 12 we have depicted this situation, but the kinetic derivation of the growth process is similar for both cases. Two paths are available to the carriers for this mass rearrangement: through (1) the surface itself; or (2) the interior of the solid.

Considering the situation involving surface diffusion and following the method outlined in Reference 3, the variation in free energy following the transfer of δN carriers between a surface position on the sphere, S, and the flat plane, F, is given by $[(\mu-\mu_h)_S-(\mu-\mu_h)_F]$. dN, where μ, μ_h are the chemical potentials of atoms and vacancies, respectively. The flux of migrating atoms is a function of this potential and the path length. Since most faces of even cubic crystals show preferred directions for surface diffusion, the flux is given by

$$j_a = -\frac{\nu}{kT}\sum_\beta \Delta_{a\beta}\frac{\delta(\mu-\mu_h)}{\delta\xi_\beta} \tag{8}$$

where

j_a, flux of surface atoms (atoms/length-time)
a,β, values for $\perp$ direction in surface plane
ξ, coordinate of directions
ν, number of surface atoms/area.

Let us assume that surface diffusion is isotropic and the facet under consideration has a circular perimeter, P. This is the most reasonable assumption for an isotropic crystal. Then, it can be shown (Fig. 12) that:

$$\delta F_S = (\gamma_F \cot\Theta - \gamma_S \csc\Theta)2\pi\sin\Psi\,\delta z$$

$$\delta F_V = \frac{\bar{\mu}-\bar{\mu}_h-\bar{\mu}_o}{\Omega} A\delta z.$$

Since the equilibrium condition is:

$$\delta F_s + \delta F_v = 0$$

one has:

$$\frac{\mu - \mu_h - \mu_o}{\Omega} = - \frac{2\pi a \sin\Psi}{A} (\gamma_F \cot \theta - \gamma_s \csc \theta).$$

Taking a constant gradient across the flat facet, then:

$$\nabla(\mu - \mu_h) = \frac{\bar{\mu} - \bar{\mu}_h - \bar{\mu}_o}{a}$$

where the bar indicates average values. With the above simplifying assumptions, Eq. (8) reduces to:

$$J = - \frac{D_s n_s}{kT} \nabla(\mu - \mu_h).$$

Now

$$\frac{dV}{dt} = J\Omega\ell'$$

and

$$dV = Adz$$

or

$$\frac{Adz}{dt} = - \frac{2\pi a \sin\Psi}{A} (\gamma_F \cot \theta - \gamma_s \csc \theta) \frac{D_s n_s}{kT} \Omega^2 \ell'. \qquad (9)$$

Taking the characteristic facet dimension as its radius $x' = a \sin\Psi$ and for $\Psi \ll \pi/2$:

$$\frac{d\Psi}{dt} = \frac{1}{a} \frac{dx'}{dt}.$$

Since

$$x'^2 \ll a, \quad A = \pi x'^2 \quad \text{and} \quad z = (a^2 - x'^2)^{1/2}$$

$$\frac{dz}{dt} = \frac{1}{z}(-2x')\left(\frac{1}{a^2 - x'^2}\right)^{1/2} \frac{dx'}{dt}.$$

Substituting into (9):

$$x'^3 dx' = 4\pi\Omega^2 \frac{D_s n_s}{kT}(\gamma_s \csc\theta - \gamma_F \cot\theta)dt.$$

But

$$\csc\theta \cong \cot\theta \text{ for } \pi/12$$

and

$$\csc\theta = a/x'.$$

Upon integration, one finally gets:

$$x'^4 = 4a^2\Omega^2 \frac{D_s n_s}{kT}(\gamma_s - \gamma_F)t. \tag{10}$$

Whenever volume diffusion predominates, the rate equation becomes:

$$\frac{dV}{dt} = J\Omega A.$$

Upon substitution and integration the result is:

$$x'^5 = 2r \frac{D_V \Omega}{kTk_1} t. \tag{11}$$

APPENDIX C

GROWTH OF NECK BETWEEN CONTACTING SPHERES

1. PARALLEL OUTWARD DISPLACEMENT OF FLAT FACETS

Let us now consider the growth of a connecting bridge between two spheres upon which flat facets have been formed in the contact area and let us assume that the process of contact formation and growth occurs by parallel displacement of facets discussed in the previous section (Fig. 13). Consider facets growing outward after a time t_1 (time for facet formation). The sink for vacancies is the sphere surface and the source is the facets in the neck region. Let us assume that the neck intercepts the facets along its entire perimeter and that each facet meets the neck radius at the same angle. If the assumption of local surface-volume equilibrium holds, the relationship between surface and volume free energy may be calculated in a manner similar to that one used previously for the growth of a single facet.

Let the facet move outward for a distance δz. For large values of α the change in surface energy may be approximated as

$$\delta F_s = -4\pi \times \gamma \sin \alpha.$$

Since there is local equilibrium between surface and bulk, it may be considered that the region directly below the surface provides material for displacement by creation of vacancies. Thus,

$$\delta F_v = \frac{\delta V}{\Omega} \mu_h - P\delta V.$$

Since the chemical potential of any region is related to standard potential and equilibrium pressure

$$\bar{\mu} = \mu_o + \bar{p}\Omega$$

$$\bar{\mu} - \bar{\mu}_h - \mu_o = -\frac{4\pi \times \gamma \sin \alpha}{\delta V}$$

where $\bar{\mu}$ and $\bar{\mu}_h$ are averaged along the area under consideration.

Let us assume that the concentration gradient of vacancies is uniform from the neck region to the outer facet perimeter over the length ℓ of the facet. Then:

$$\nabla(\mu - \mu_h) = \frac{\mu - \mu_h - \mu_o}{\ell} .$$

The diffusive flux of atoms to facet is:

$$J = - \frac{D_s n_s}{kT} \nabla(\mu - \mu_h)$$

and rate of transport is:

$$\frac{dV}{dt} = J\Omega P.$$

Upon substitution of the proper terms for the flux rate expression for parallel facet displacement by surface diffusion is obtained. Table II summarizes the results for both volume and surface diffusion.

2. ROTATIONAL DISPLACEMENT OF FACETS

Facets may also grow by a rotational displacement around two fulcra situated along the boundary between the flat and the curved portion of the spheres (Fig. 14). In this instance the contact angle is not constant.

Let us consider two different cases in which (1) the source of material is grain boundary and the sink the neck region or grain interior, and (2) the source is the sphere surface and the sink the neck region. For both models the existence of a fillet as a vacancy source is not required. The contact angle is not the equilibrium angle and must change with neck growth. Assuming again that surface-volume equilibrium holds, the derivation of the rate expressions follows in a manner similar to the previous cases.

The rate expressions are:

$$\left(\frac{dV}{dt}\right)_B = J\Omega A$$

$$\left(\frac{dV}{dt}\right)_{AB} = J\Omega P.$$

Upon substitutions of proper flux expressions, the values listed in Table III are obtained.

TABLE II

GROWTH OF CONTACT BETWEEN SOLID SPHERES
BY PARALLEL DISPLACEMENT OF FLAT SURFACES

Vacancy source	Facet surface	Facet surface
Sink	Sphere surface	Sphere surface
Mechanism	Surface diffusion	Surface diffusion
dV/dt	$\pi \ell \cos\alpha (2x + \ell \sin\alpha) \delta x$	$2\pi \ell x \cos\alpha dx$
Perimeter	Constant $\propto a$	Constant $\propto a$
Area	--	--
$\Delta(\mu - \mu_n)$	$-\frac{\Omega 4\pi x \gamma \sin\alpha}{\delta V}$	$-\frac{\pi 4 \Omega x \gamma \sin\alpha}{\delta V}$
Path	ℓ	Constant $\propto a$
Rate expression	$A \log x - Bx = kT$	$\left(\frac{x}{a}\right)^2 = \frac{D_S n_S \Omega^2 \gamma \sin\alpha}{kT\ \ell a \cos^2\alpha}$
Scaling law	4	4

TABLE III

GROWTH OF CONTACT BETWEEN SOLID SPHERES BY ROTATIONAL DISPLACEMENT OF FACETS

Vacancy source	Grain interior	Surface	Neck surface	Neck surface
Sink	Grain boundary	Grain boundary	Sphere surface	Sphere surface
Mechanism	Bulk diffusion	Grain boundary diffusion	Bulk diffusion	Surface diffusion
dV/dt	$\pi x^3 \frac{dx}{dt}$	$\pi x^3 \frac{dx}{dt}$	$\frac{4\pi x^3}{a} \frac{dx}{dt}$	$\frac{4\pi x^3}{a} \frac{dx}{dt}$
Perimeter	--	$2\pi x$	--	$4\pi x$
Area	πx^2	--	$3\pi x^2$	--
$\Delta(\mu - \mu_h)$	$\frac{2\gamma\Omega a}{x^2}$	$\frac{2\gamma\Omega a}{x^2}$	$\frac{2\gamma a\Omega}{3x^2}$	$\frac{2\gamma a\Omega}{3x^2}$
Path	Constant $\propto a$	$\propto x$	$\propto a$	$\propto a$
Rate expression	$\frac{x^4}{a^4} = \frac{\gamma D_V \Omega \gamma t}{kT\ ca^3}$	$\left(\frac{x}{a}\right)^6 = \frac{24 D_S n_S \Omega^2 \gamma t}{kT\ ca^4}$	$\left(\frac{x}{a}\right)^4 = \frac{2 D_V \gamma t}{kT\ a^3}$	$\left(\frac{x}{a}\right)^5 = \frac{8 D_S \Omega^2 \gamma t}{kT\ a^4}$

APPENDIX D

LIST OF SYMBOLS

A	area
$Å$	Avagadro constant
D_S	surface diffusion constant
D_V	volume diffusion constant
M	molecular weight
R	gas constant
T	absolute temperature
V	volume
a	sphere radius
c	proportionality constant for path
f	fugacity
k	Boltzmann constant
ℓ	facet length
ℓ'	facet perimeter
m	scaling exponent
n	rate exponent
n_s	atomic surface density
p	vapor pressure
t	time
t_o	yime of facet appearance
x	contact neck radius

x_o	neck radius at t_o
x'	facet radius
dz	virtual displacement distance
α	angle between facet normal and contact radius
γ	surface energy
θ	angle between facet face and sphere surface
μ	chemical potential of atom
μ_o	equilibrium chemical potential
μ_h	chemical potential of vacancy
Ψ	angle intercepted by facet radius
Ω	atomic volume

REFERENCES

1. Kuczynski, G. C., Trans. AIME 185, 169 (1949).

2. O'Bryan, H. M., Jr. and G. Parravano, "Sintering of Rutile," in: Powder Metallurgy, W. Leszynski, ed., Interscience Publishers (1961).

3. Herring, C., "Surface Tension as a Motivation for Sintering," in: Physics of Powder Metallurgy, Kingston, ed., McGraw-Hill Book Company (1951).

4. Buessem, W. R. and S. R. Butler, "Defect in TiO_2," in: Kinetics of High-Temperature Processes, W. D. Kingery, ed., Wiley (1959).

5. Kofsted, P., K. Hauffe, and H. Kjollesdal, Acta Chem. Scand. 12, 239 (1958).

6. Haul, R., D. Just and G. Dumbgen, "Sauerstoffdiffusion in Oxyden," in: Reactivity in Solids, de Boer, ed., Elsevier (1961).

7. Kuczynski, G. C., L. Abernathy and J. Allan, "Sintering Mechanisms of Aluminum Oxide," in: Kinetics of High-Temperature Processes, W. D. Kingery, ed., Wiley (1959).

8. Ackermann, R. J., and R. J. Thorn, Progress in Ceramic Science 1, Pergamon (1961).

9. Lewis, G. N. and M. Randall, Thermodynamics, Revised Edition, McGraw-Hill Book Company (1961).

10. Kingery, W. D., J. Appl. Phys., 31, 833 (1960).

11. Herring, C., in: Structure and Properties of Solid Sufaces, R. Gomer and C. S. Smith, ed., University of Chicago Press (1953).

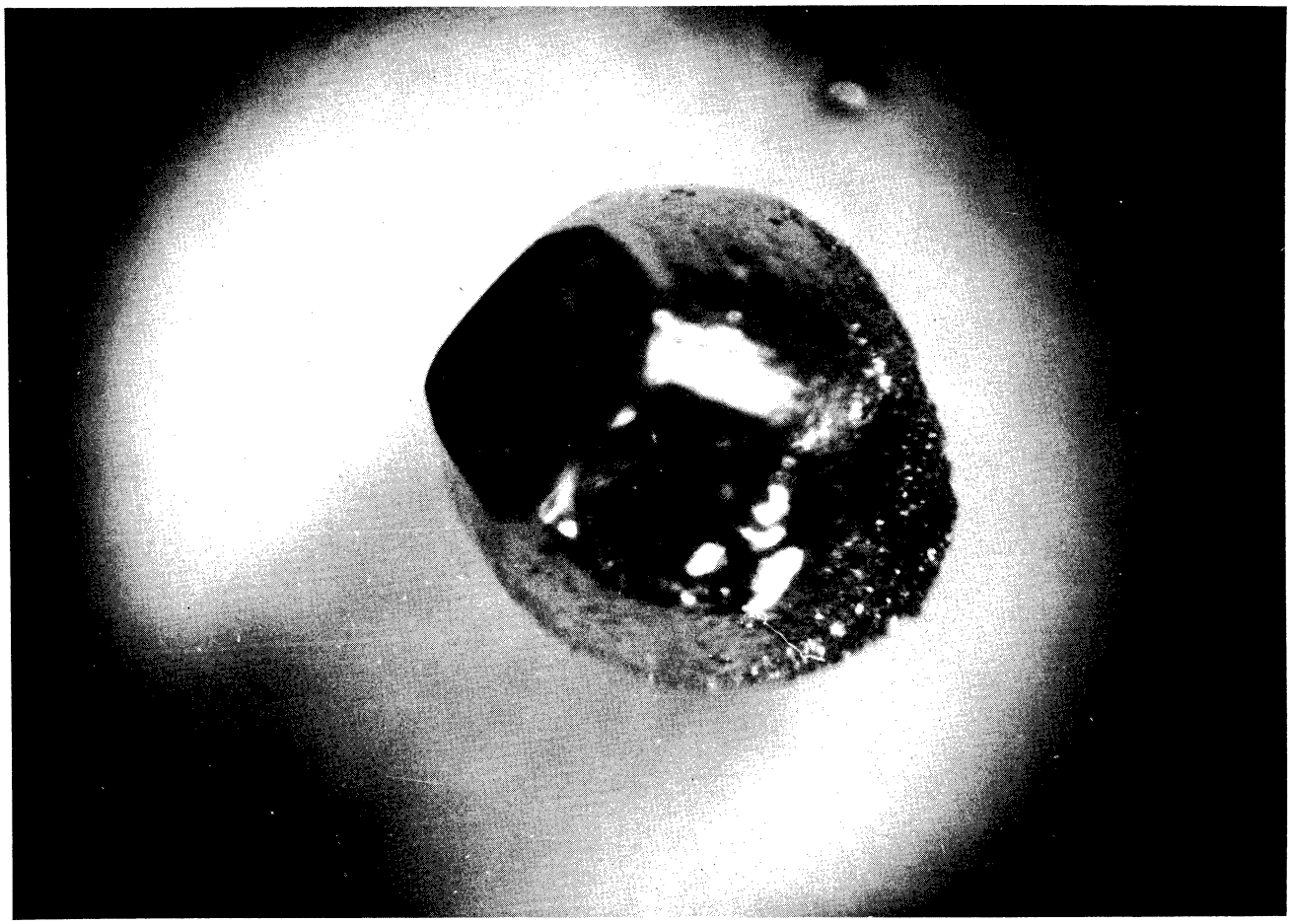

Fig. 1. Faceted TiO_2 single crystal sphere sintered in low oxygen atmosphere (p_{O_2} = .02) at 1250°C for 800 minutes 60X.

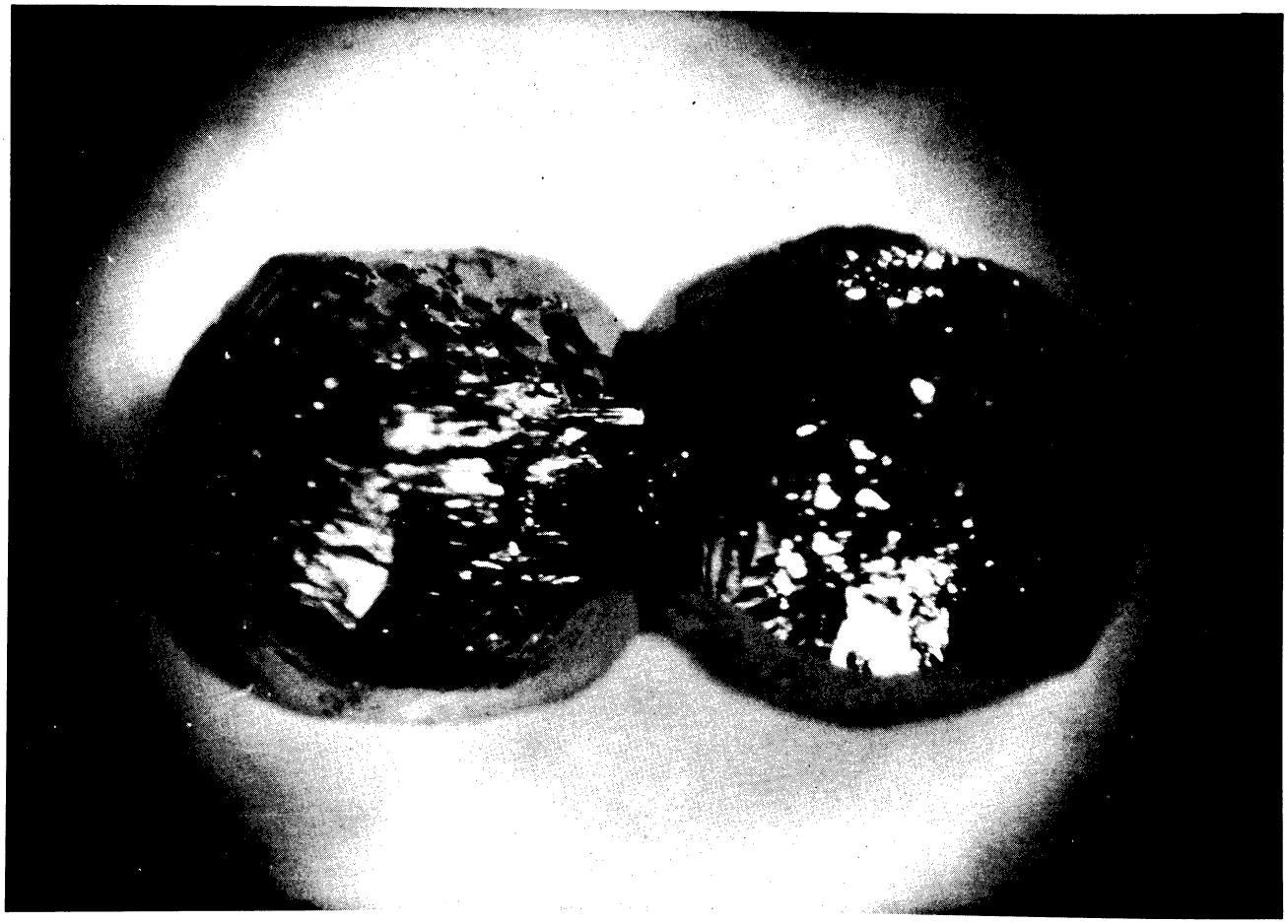

Fig. 2. TiO_2 single crystal spheres sintered in reducing atmosphere (p_{H_2}/p_{H_2O} = 10) at 1050°C for 800 minutes. 60X.

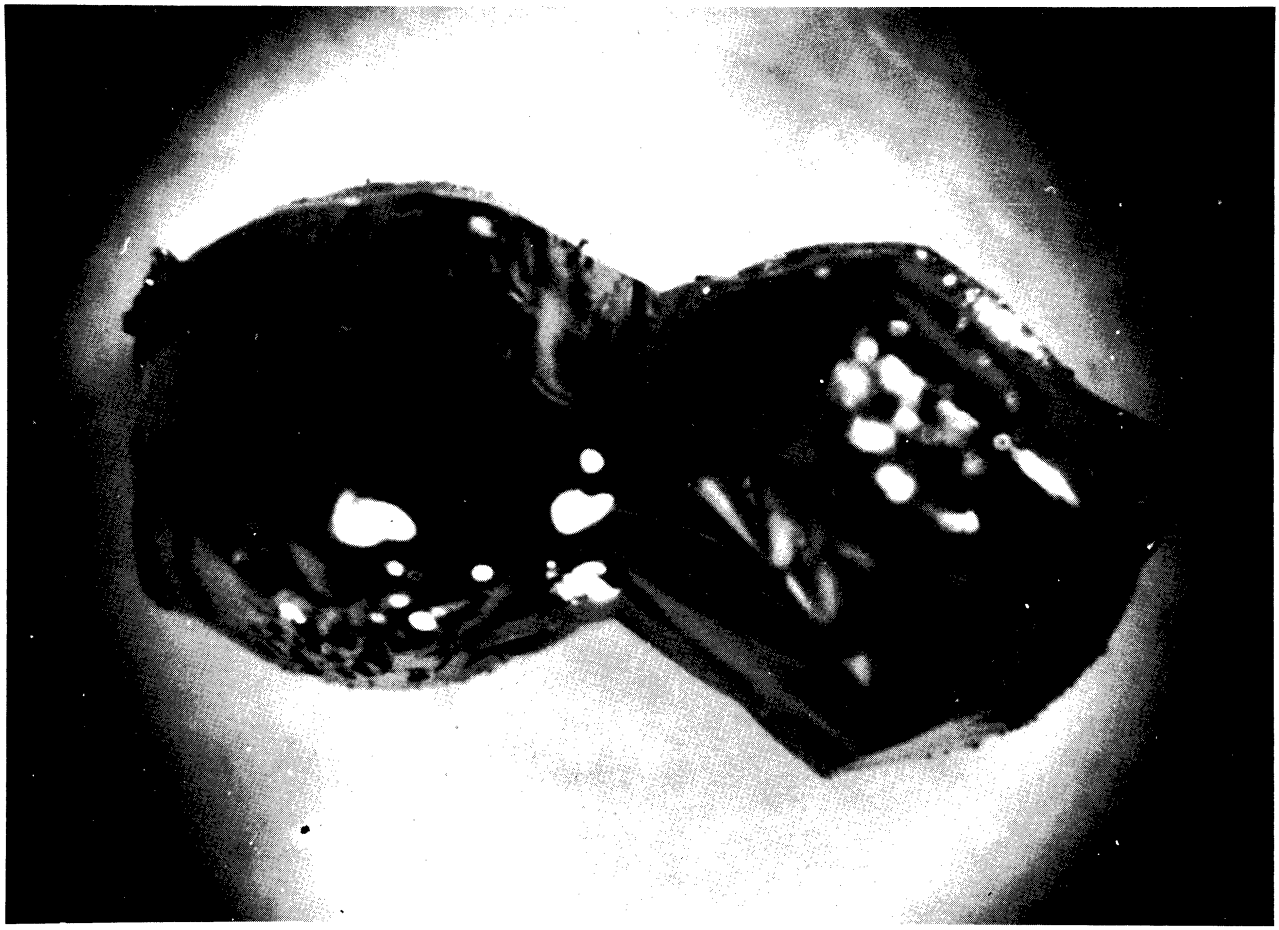

Fig. 3, TiO_2 single crystal spheres sintered in reducing atmosphere (p_{H_2}/p_{H_2O} = 10) at 1200°C for 600 minutes. 60X.

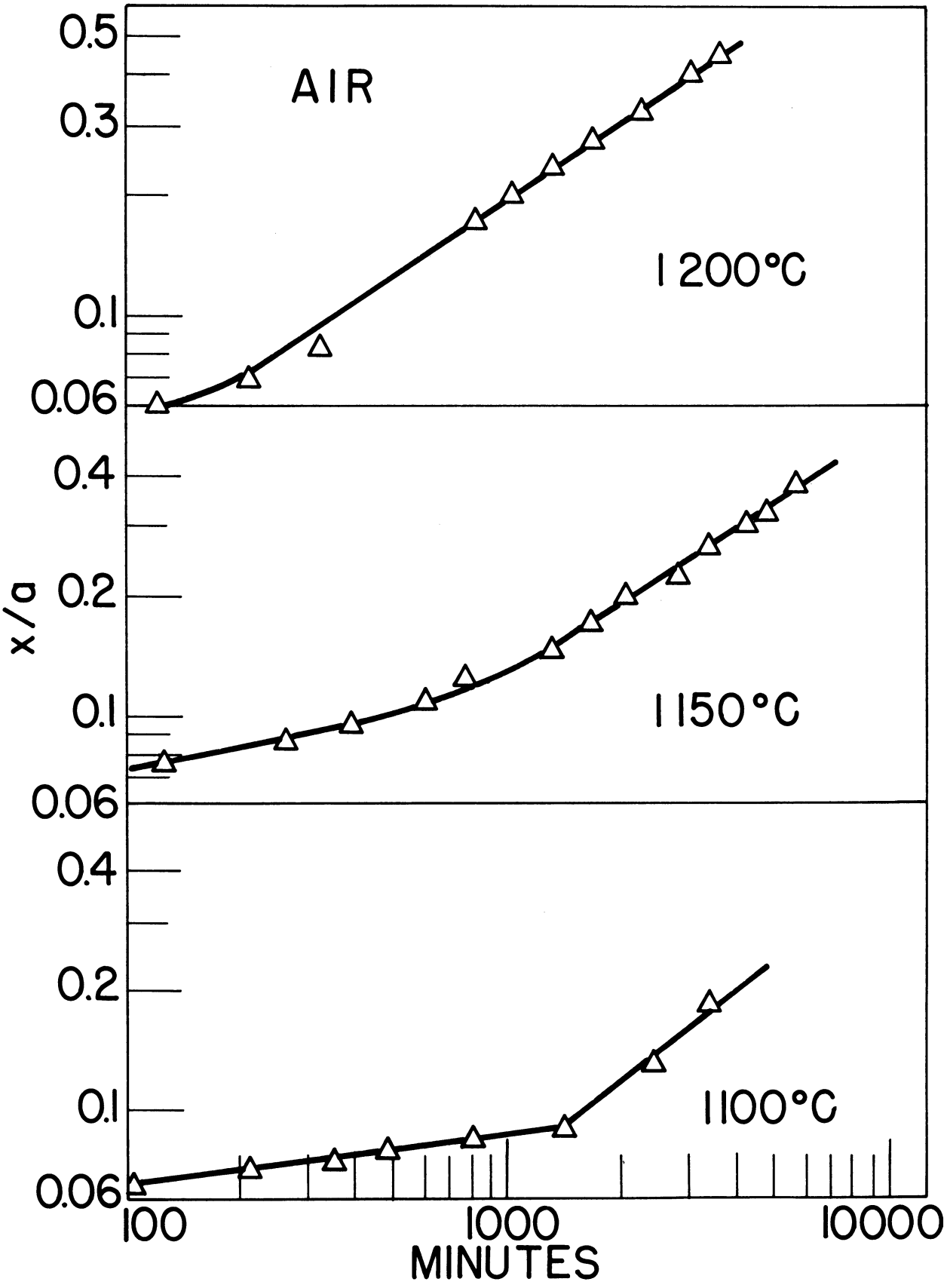

Fig. 4. Time and temperature dependence of the ratio of neck-to-particle radius for 1 mm diameter TiO_2 spheres sintered in air.

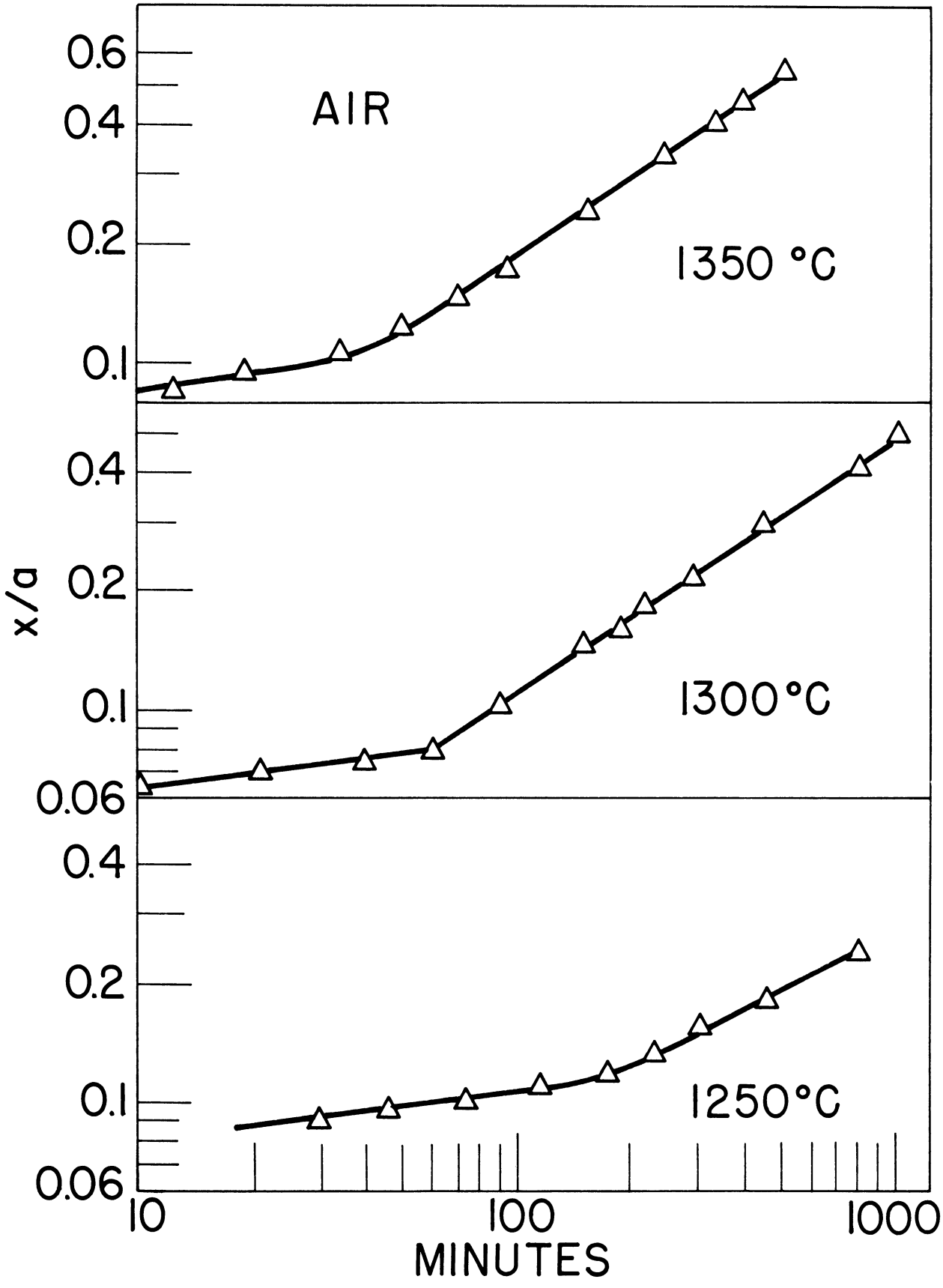

Fig. 5. Time and temperature dependence of the ratio of neck-to-particle radius for 1 mm diameter TiO_2 spheres sintered in air.

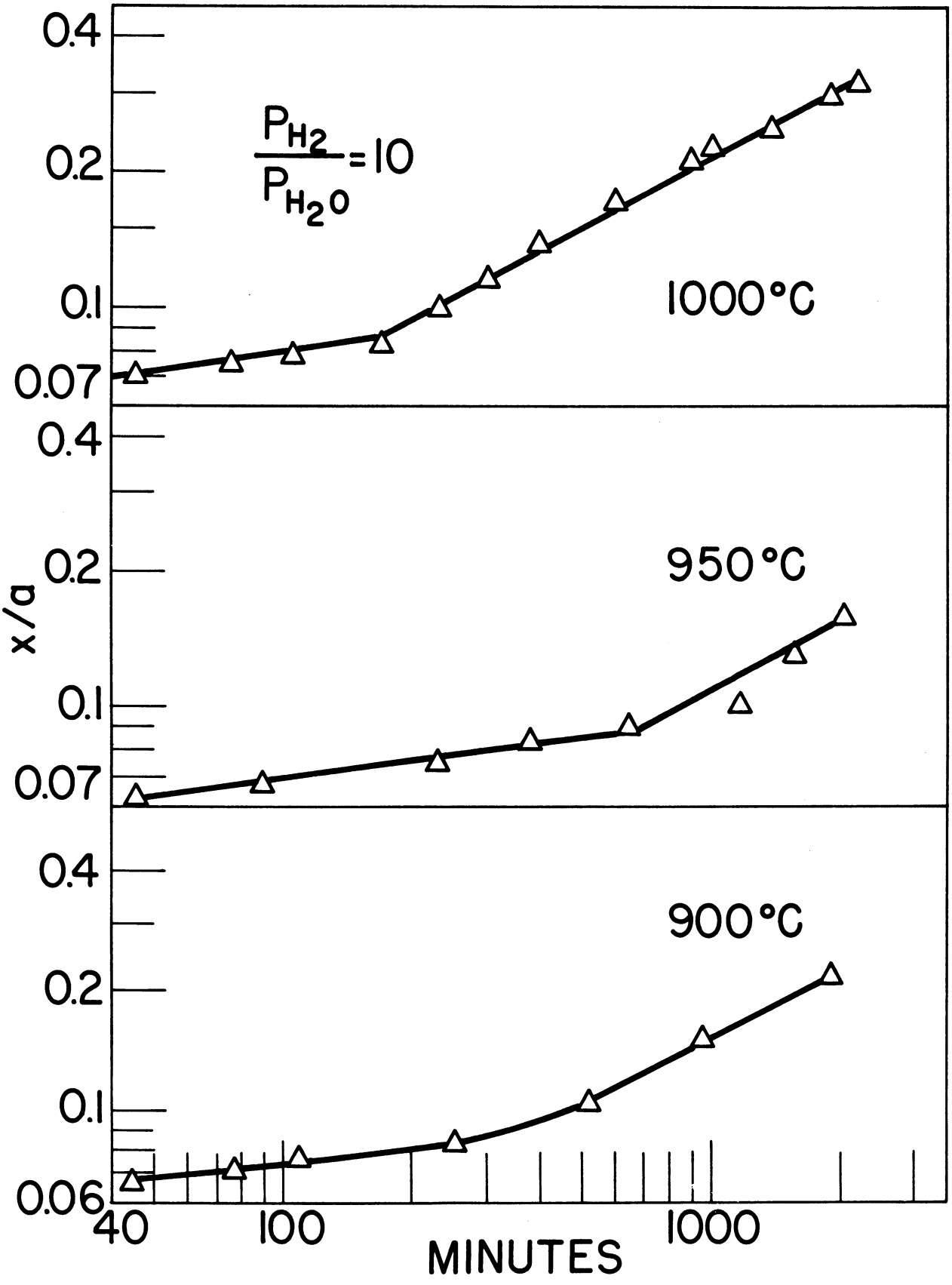

Fig. 6. Time and temperature dependence of the ratio of neck-to-particle radius for 1 mm diameter TiO_2 spheres sintered in reducing atmosphere (p_{H_2}/p_{H_2O} = 10).

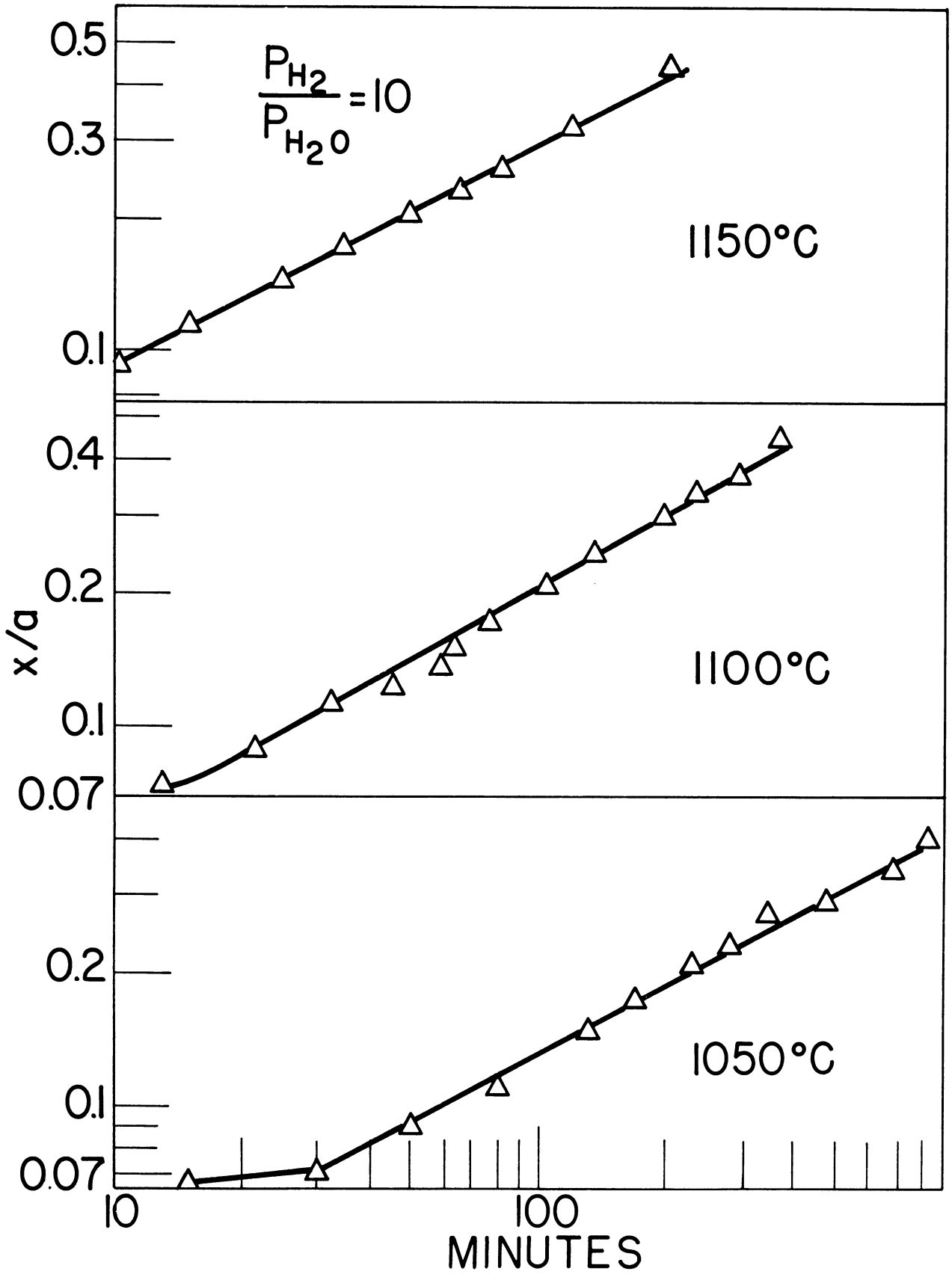

Fig. 7. Time and temperature dependence of the ratio of neck-to-particle radius for 1 mm diameter TiO_2 spheres sintered in reducing atmosphere (p_{H_2}/p_{H_2O} = 10).

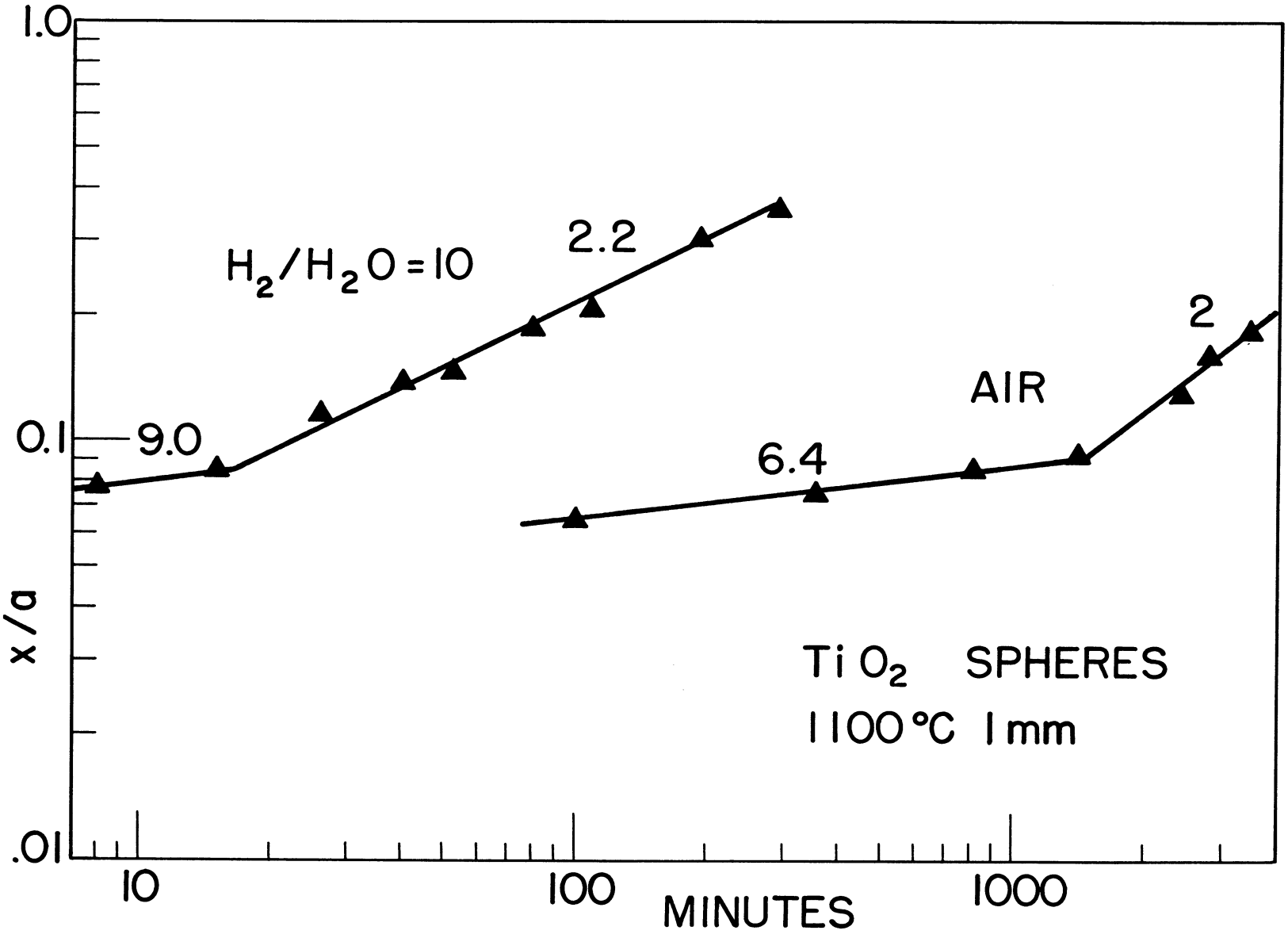

Fig. 8. Comparison of sintering rates in air and reducing atmosphere (p_{H_2}/p_{H_2O} = 10) at 1100°C for 1 mm diameter TiO_2 single crystal spheres.

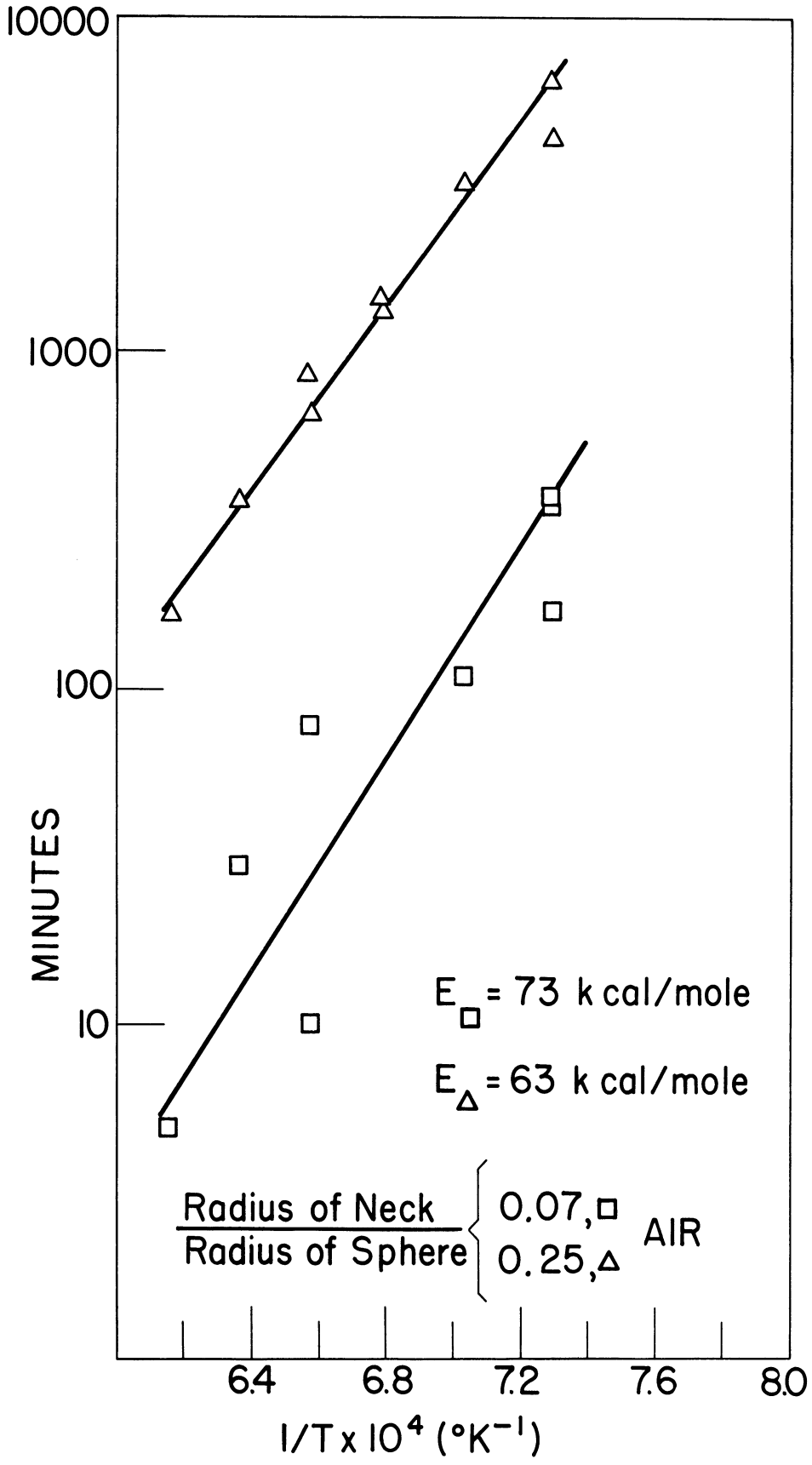

Fig. 9. Time for a ratio of neck-to-particle radius x/a = 0.07 initial stage and x/a = 0.25 second stage as a function of absolute temperature for 1 mm diameter TiO_2 spheres sintered in air.

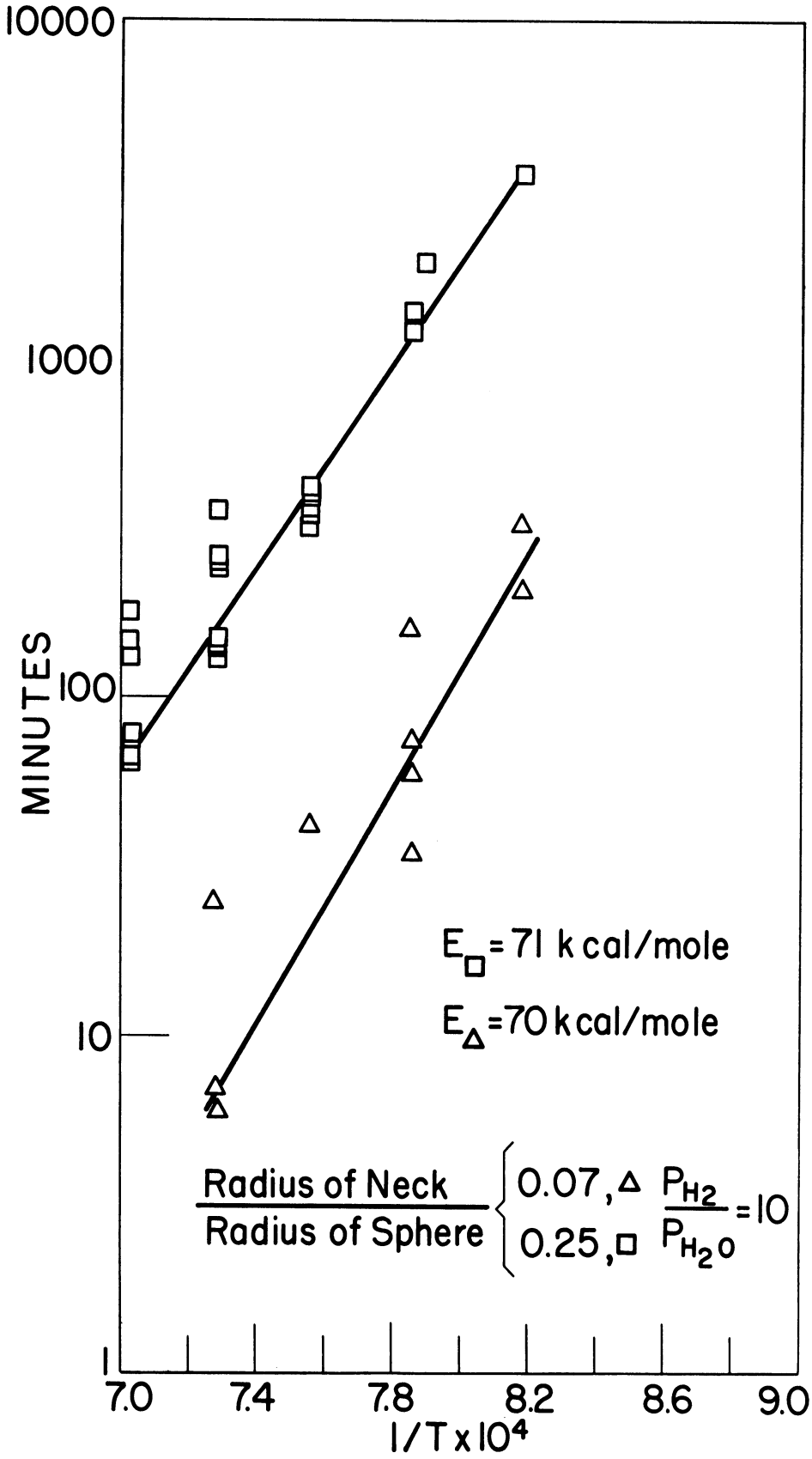

Fig. 10. Time for a ratio of neck-to-particle radius x/a = 0.07 initial stage and x/a = 0.25 second stage as a function of absolute temperature for 1 mm diameter TiO_2 spheres sintered in reducing atmosphere (p_{H_2}/p_{H_2O} = 10).

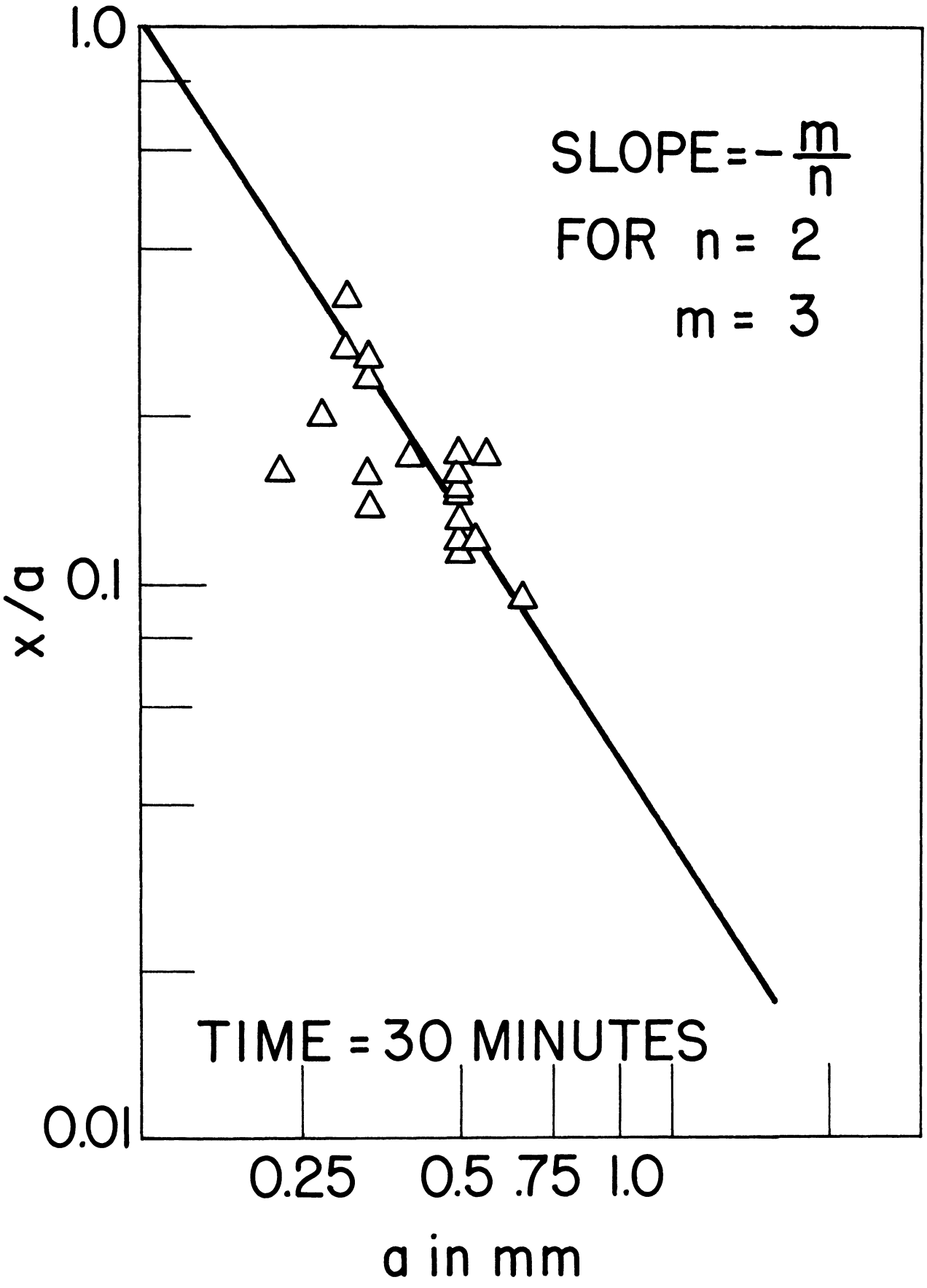

Fig. 11. Effect of particle size for sintering of TiO_2 single crystal sphere at 1150°C in reducing atmosphere.

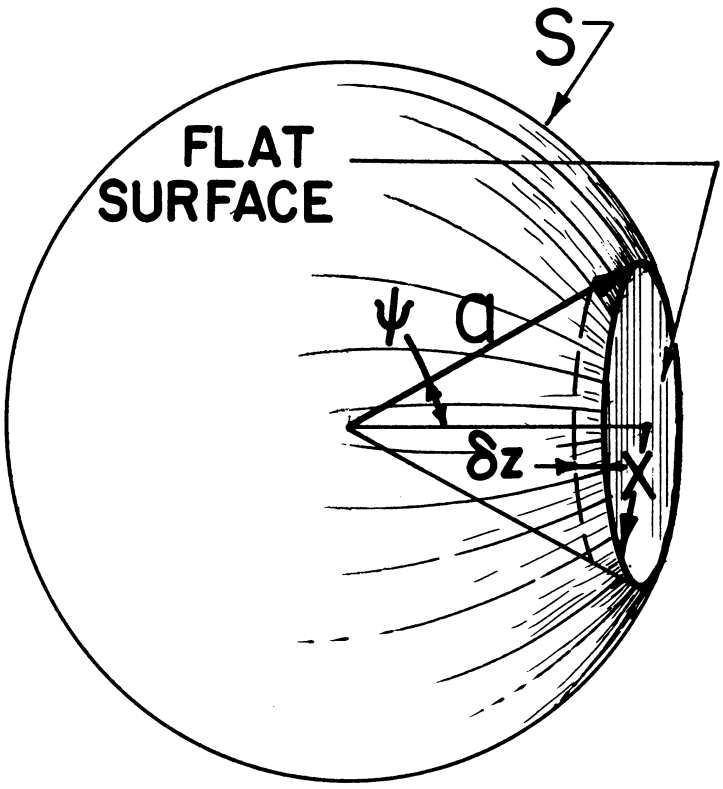

Fig 12. Growth of a flat facet on a spherical surface by parallel displacement.

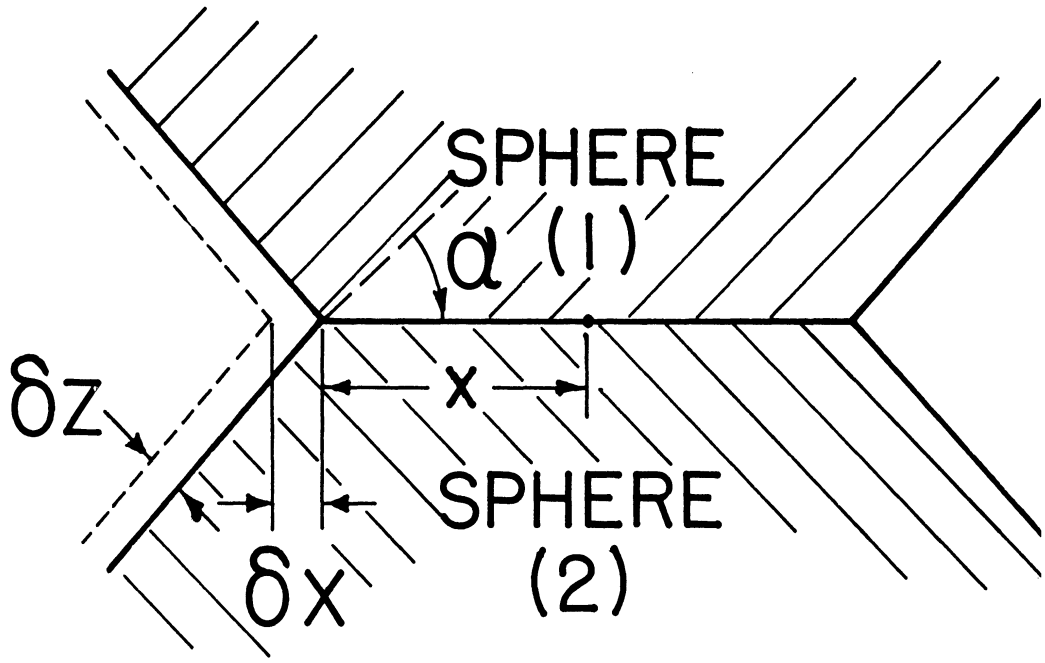

Fig. 13. Formation and growth of contact between two spherical surfaces flattened in the contact area by facet growth, occurring by parallel displacement of itself.

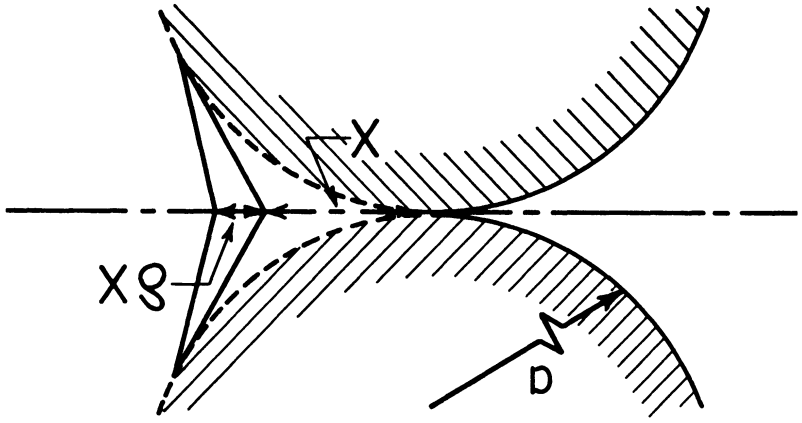

Fig. 14. Formation and growth of contact between two spherical surfaces flattened in the contact area by facet growth, occurring by rotational displacement around a fulcrum.

DISTRIBUTION LIST

(One copy unless otherwise noted)

Air Force Office of Scientific
Research
Washington 25, D.C.
Attn: Solid State Sciences Division 3
Attn: Technical Library (SRGL) 2

ASTIA 10
Arlington Hall Station
Arlington 12, Virginia
Attn: TIPCR

Commander 2
Army Rocket & Guided Missile Agency
Redstone Arsenal, Alabama
Attn: ORDXR-OTL

RAND Corporation 2
1700 Main Street
Santa Monica, California

ARDC
Andrews Air Force Base
Washington 25, D.C.
Attn: RDRS

EOAFRD, ARDC
47 Cantersteen
Brussels, Belgium

HQ, USAF
Washington 25, D.C.
Attn: AFDRT

ARL
Building 450
Wright-Patterson Air Force Base
Ohio
Attn: Technical Library

WADD
Wright-Patterson Air Force Base
Ohio
Attn: WWAD

WADD
Materials Central
Wright-Patterson Air Force Base, Ohio
Attn: Metals & Ceramics Lab.
Attn: Physics Lab.
Attn: Materials Information Branch

Institute of Technology Library
MCLI-LIB, Building 125, Area B
Wright-Patterson Air Force Base, Ohio
Attn: AU

ARL
AFRD
Wright-Patterson Air Force Base, Ohio
Attn: Metallurgy
Attn: Solid State Physics

AFOSR
Holloman Air Force Base, New Mexico
Attn: SRLTL

AFCRL
L. G. Hanscom Field, Bedford, Mass.
Attn: CRRELA

AFFTC
Edwards Air Force Base, California
Attn: FTCTL

AEDC
Arnold Air Force Station, Tennessee
Attn: AEOIM

AFSWC
Kirtland Air Force Base, New Mexico
Attn: SWOI

Office of the Chief of Research
and Development
Department of the Army
Washington 25, D.C.
Attn: Scientific Information

DISTRIBUTION LIST (Continued)

Army Research Office
Box CM, Duke Station
Durham, North Carolina
Attn: CRD-AA-IP

Commanding Officer
Ordnance Materials Research Office
Watertown Arsenal
Watertown 72, Massachusetts
Attn: PS&C Div.

Commanding Officer
Watertown Arsenal Laboratories
Watertown 72, Massachusetts
Attn: Technical Reports Section

Commander
Signal Corps Engineering Laboratory
Fort Monmouth, New Jersey
Attn: SIGFM/EL-RPO

Director
U. S. Naval Research Laboratory
Washington 25, D.C.
Attn: Library

Department of the Navy
Office of Naval Research
Washington 25, D.C.
Attn: Code 423
Attn: Code 421

Officer in Charge
Office of Naval Research
Navy No. 100
Fleet Post Office
New York, New York

Commanding Officer
Naval Radiological Defense
Laboratory
San Francisco Naval Shipyard
San Francisco 24, California

Dr. D. F. Bleil
Associate Technical Director for
Research
U. S. Naval Ordnance Laboratory
White Oak, Silver Spring, Maryland

National Aeronautics & Space Agency
1520 H Street, N.W.
Washington 25, D.C.
Attn: Library

Ames Research Center (NASA)
Moffett Field, California
Attn: Technical Library

High Speed Flight Station (NASA)
Edwards Air Force Base, California
Attn: Technical Library

Langley Research Center (NASA)
Langley Air Force Base, Virginia
Attn: Technical Library

Lewis Research Center (NASA)
21000 Brookpark Road
Cleveland 35, Ohio
Attn: Technical Library

Wallops Station (NASA)
Wallops Island, Virginia
Attn: Technical Library

Division of Research
U.S. Atomic Energy Commission
Division Office
Washington 25, D.C.

U.S. Atomic Energy Commission
Library Branch
Technical Information Division, ORE
P. O. Box E
Oak Ridge, Tennessee

DISTRIBUTION LIST (Concluded)

Major John Radcliffe
ANP Office
U.S. Atomic Energy Commission
Washington 25, D.C.

Oak Ridge National Laboratory
P. O. Box P
Oak Ridge, Tennessee
Attn: Central Files

Brookhaven National Laboratory
Upton, Long Island, New York
Attn: Research Laboratory

Argonne National Laboratory
9700 S. Cass Avenue
Argonne, Illinois
Attn: Library

Document Custodian
Los Alamos Scientific Laboratory
P. O. Box 1663
Los Alamos, New Mexico

Ames Laboratory
Iowa State College
P. O. Box 14A, Station A
Ames, Iowa

Knolls Atomic Power Laboratory
P. O. Box 1072
Schenectady, New York
Attn: Document Librarian

National Science Foundation
1901 Constitution Avenue, N.W.
Washington 25, D.C.

National Bureau of Standards Library
Room 203, Northwest Building
Washington 25, D.C.

Director
Office of Technical Services
Department of Commerce
Technical Reports Branch
Washington 25, D.C.

Chairman
Canadian Joint Staff
2450 Massachusetts Avenue, N.W.
Washington, D.C.
Attn: DRB/DSIS

Defense Research Member
Canadian Joint Staff
Director of Engineering Research
Defense Research Board
Ottawa, Canada
Attn: Mr. H. C. Oatway

Institute of the Aeronautical Sciences
2 East 64th Street
New York 21, New York
Attn: Librarian